32nd Electric Vehicle Symposium (EVS32)
Lyon, France, May 19 - 22, 2019

Development of a self-adaptive cycle ageing model for Li-ion batteries using Machine Learning methods

M.Lucu[1,2,*], J.A. López-Ibarra[1,2], E. Martinez-Laserna[1], I. Gandiaga[1], H. Camblong[2,3]

[1]*IK4-Ikerlan Technology Research Centre, Energy Storage and Management Area. P° J.M. Arizmendiarrieta, 2. 20500 Arrasate-Mondragón, Spain. *mlucu@ikerlan.es*

[2]*University of the Basque Country (UPV/EHU), Department of Systems Engineering & Control. Europa Plaza, 1. 20018 Donostia-San Sebastian, Spain*

[3]*ESTIA Research, Ecole Supérieur des Technologies Industrielles Avancées (ESTIA), Technopole Izarbel, 64210 Bidart, France*

Summary

Conventional Li-ion ageing models require a large amount of time and cost-intensive laboratory tests to provide accurate predictions in realistic operating conditions. Concurrently, industry progress into digital transformation, making considerable efforts in data collection. This implies the forthcoming availability of a significant amount of real-world battery operation data. In this context, self-adaptive ageing models, able to learn from in-field battery operation data and adapt lifetime estimations to the real life become an interesting solution to reduce laboratory labours. Based on extensive experimental tests at static and dynamic conditions, a self-adaptive capacity loss model is proposed under the Gaussian Process framework.

Keywords: Lithium battery, Battery cycle life, Modeling, Digitalization, Fleet.

1. Introduction

Lithium-ion (Li-ion) technology has gained market share until becoming the principal energy storage solution for many industrial applications, mainly due to its high efficiency and high specific energy and power. However, Li-ion batteries still expensive, and their performance declines over time and use, which threatens its competitiveness against more affordable solutions [1]. The development of ageing models allow to predict the degradation of Li-ion batteries, providing useful information to improve the sizing of battery packs, adjust warranty periods and assist business case definition.

Different kinds of ageing models were proposed in the literature, involving empirical, semi-empirical and physics-based models [2]. Nevertheless, a main inconvenience for the development of such a conventional ageing models is the huge amount of laboratory tests needed to verify their accuracy at realistic operating conditions. Actually, all these conventional models are typically parametrised using laboratory tests carried out at constant ageing conditions [3]. Furthermore, extensive validation procedures involving constant ageing conditions, slowly varying dynamic conditions and realistic ageing profiles are recommended to surround accurate lifetime predictions in a context of real-world operation [4]. However, even such validation procedures could difficultly ensure accurate predictions for a large diversity of dynamic or realistic profiles, which may involve different ageing rates due to the effect of the path dependence [5].

A possible solution to reduce the number of laboratory tests is to work on the development of self-adaptive ageing models. In this paper, a self-adaptive model is understood as a model able to update or correct itself to fit better the newly available data samples. Following this approach, reduced laboratory tests could be used to develop a preliminary ageing model. Further, once the battery pack is implemented and operating, in-field data could allow to update the preliminary ageing model. In this way, the ageing model would be continuously upgraded, improving prediction accuracy, and providing useful information for predictive maintenance, adaptive energy management strategies or business case redefinition.

In a previous publication, a critical review on self-adaptive ageing models for Li-ion batteries was presented, in which the Gaussian Process (GP) models were identified as most promising candidates [6]. In fact, beyond their ability to perform probabilistic, relatively robust and computationally acceptable predictions, these models enjoy the very interesting advantage of being nonparametric: in other words, the complexity of these models depends on the amount of training data. In the context of Li-ion ageing prediction, this implies:

- *A progressive spread of the operating window of the model.* Each time a new data sample related to previously unobserved operating conditions is included into the training set, additional knowledge is obtained about the influence of stress-factors on ageing. The resulting models are able to provide an increasingly comprehensive picture of the ageing of Li-ion batteries.
- *A higher level of specialisation of the model.* The preliminary ageing model developed from the laboratory data could be upgraded including new training data extracted from in-field operation. In-field data encodes the intrinsic operating profiles of each applications. This implies the possibility to move from a generic ageing model to specialised models tailored to specific applications.

This paper focuses on the modelling of the cycle ageing of Li-ion batteries, considering the effect of the cycling temperature, Depth-of-Discharge (DOD) and Middle-State of Charge (SOC). Section 2 describes the experimental ageing tests carried out in order to produce the ageing data. Section 3 details the processing of the raw data. Section 4 introduces the theoretical background of the GP framework. In Section 5, the selection of the inputs and kernel functions are justified. Section 6 states the obtained results for both static and dynamic operating conditions. Section 7 discusses the obtained results and outlines the limitations of the study and further works. Finally, Section 8 closes the study depicting the main conclusions.

2. Experimental ageing data

Experimental ageing tests were performed on NMC/graphite 20Ah pouch cells, in a temperature-controlled environment. Periodical check-up experiments were carried out at 25°C to evaluate the capacity of the cells every 100 Full-Equivalent-Cycles (FEC). Between each capacity test, a total of 95 cells from the same manufacturing batch were tested at the corresponding temperature, DOD and Middle-SOC levels (specified in Table 1). For these ageing tests, the cycling temperature, DOD and Middle-SOC level of every cell remained unchanged during the whole duration of the tests, which were 3750 FEC for the longest test.

Table 1. Cycle ageing test matrix

Temperature [°C]	DoD [%]	100	80	65	50			35	20					10		
	MidSOC [%]	50	50	50	65	50	35	50	80	65	50	35	20	80	65	20
25		CELL001 CELL002 CELL003	CELL004 CELL005 CELL006 CELL007 CELL008 CELL009 CELL010 CELL011	CELL012 CELL013 CELL014		CELL015 CELL016 CELL017		CELL018 CELL019 CELL020			CELL021 CELL022 CELL023					
35		CELL030 CELL031 CELL032	CELL033 CELL034 CELL035 CELL036 CELL037 CELL038 CELL039 CELL040	CELL041 CELL042 CELL043	CELL044 CELL045 CELL046	CELL047 CELL048 CELL049 CELL050 CELL051 CELL052 CELL053 CELL054	CELL055 CELL056 CELL057	CELL058 CELL059 CELL060	CELL061 CELL062 CELL063	CELL064 CELL065 CELL066	CELL067 CELL068 CELL069	CELL070 CELL071 CELL072	CELL073 CELL074 CELL075	CELL076 CELL077 CELL078	CELL079 CELL080 CELL081	CELL082 CELL083 CELL084
45		CELL100 CELL101 CELL102	CELL103 CELL104 CELL105 CELL106 CELL107 CELL108 CELL109 CELL110	CELL111 CELL112 CELL113		CELL114 CELL115 CELL116		CELL117 CELL118 CELL119			CELL120 CELL121 CELL122					

As the battery cycling conditions are barely constant over time, 2 cells were cycled at dynamic temperature, DOD, Middle-SOC and charging and discharging C-rate levels. These cells were reserved for the validation of the developed model, and the obtained capacity curves and the corresponding dynamic operating profiles are detailed in Section 6.2.

3. Data pre-processing

In the context of data-driven or empirical modelling, the data used for the training and validation of the model must be analysed prior to any modelling task, in order to remove the data involving potential errors and possibly separate the components which are desired to be modelled from those which deserve to be discarded. For the modelling of Li-ion battery ageing, a deep electrochemical understanding provides a solid background to make this task easier. In this section, the raw data obtained from the experimental tests is analysed and processed for the further modelling stage.

In the experimental data, a capacity rise phenomenon appears on the Beginning of Life (BOL) phase of the tested cells. According to the literature, the capacity rise could be induced by a slow, compensating flow of active lithium between the passive and the active part of the anode, where the passive part represents the geometric excess anode with respect to the cathode [7]. Despite a deep research in the literature, no clear relation was found between the initial capacity rise and any ageing mechanism, and it was assumed that the initial capacity rise phenomenon does not have any influence on the posterior ageing trend of the cells. Accordingly, the data corresponding to the capacity rise was discarded for the development of the ageing model. During the data pre-processing phase the maximal capacity point of each cell was designated as the BOL point, and assigned to the 'zero Ah-throughput' state.

After a regular decline of the capacity, some cells showed a clear acceleration of the ageing rate. The post-mortem analyses performed in all cells below 80% of the remaining capacity revealed metallic lithium deposed on the whole surface of the anode. Therefore, the sudden capacity drop was linked to the occurrence of lithium deposition. The current study presents a partial cycle ageing model, which does not take into account the effect of the charging and discharging currents on ageing, which are strongly related to the lithium deposition phenomenon. Consequently, the data samples corresponding to sudden capacity drop phenomena were discarded from the modelling dataset in the current study. Furthermore, some unexpected ageing behaviours were detected, notably some one-off lower or higher capacity data points, which were allocated to measurement or procedural errors during the capacity tests. These data samples were also removed from the modelling dataset. The remaining ageing data obtained after the pre-processing stage is visualised in Figure 1.

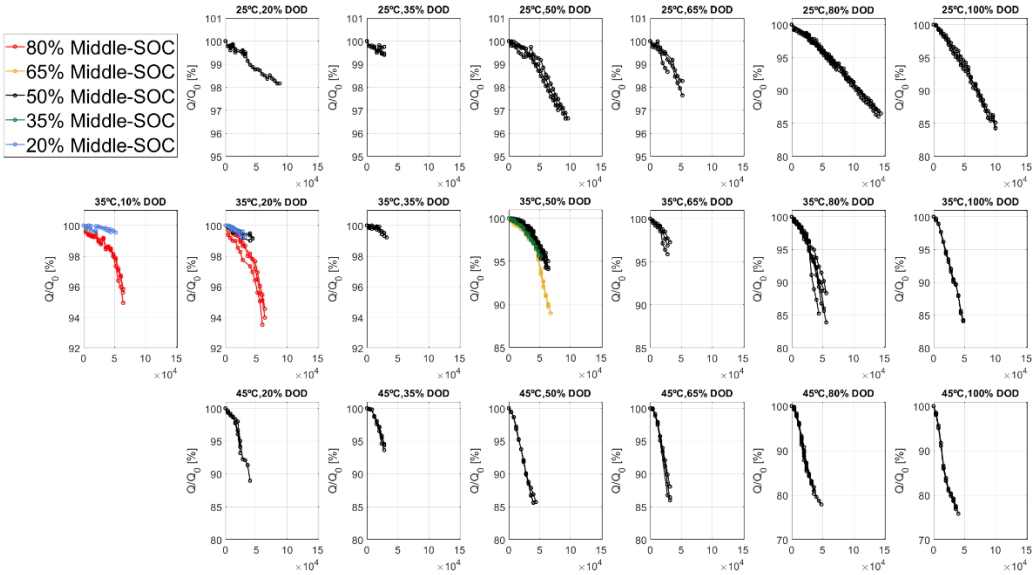

Figure 1. Actual capacity normalised to maximum value (Q_{max}), obtained after the pre-processing phase of static ageing tests. Notice that, for clarity purposes, the y-axis scale is varying from a subplot to another.

4. Gaussian Process theory

This section aims at giving a brief overview of Gaussian Process models. The GP is a random process, *i.e.* a random entity whose realisation is a function $f(x)$ instead of a single value. Rather than assuming a parametric form for the function to fit the data, $f(x)$ is assumed to be a sample of a Gaussian random process distribution. Since the GP is a nonparametric model, even when a lot of observations have been added, the model should always be capable to fit the data.

A GP is fully determined by its mean and covariance functions, which express the expected behaviour of the model when the prediction inputs diverge from the inputs observed in training. The covariance function, also called *kernel*, gives the information about how relevant is one target observation y of the training dataset to predict the output y^*, in the basis of the similarity between their respective input values x and x^*.

The mean and covariance functions depend on some hyperparameters θ, which must be learned from the training dataset. From the GP point of view, the mean and covariance function selection and learning the corresponding hyperparameters are the main tasks which must be carried out during the training phase. Hyperparameters are typically estimated by the maximisation of the marginal likelihood logarithm [8]. The GP predictive equations are expressed in equations (1), (2) and (3).

$$\boldsymbol{f}_*|X,y,X_* \sim \mathcal{N}(\bar{\boldsymbol{f}}_*, cov(\boldsymbol{f}_*)) \tag{1}$$

$$\bar{\boldsymbol{f}}_* = \boldsymbol{m}(X_*) + K(X_*,X)[K(X,X) + \sigma_n^2 I]^{-1}(y - \boldsymbol{m}(X)) \tag{2}$$

$$cov(\boldsymbol{f}_*) = K(X_*,X_*) - K(X_*,X)[K(X,X) + \sigma_n^2 I]^{-1}K(X,X_*) \tag{3}$$

where $\boldsymbol{f}_*$, $\bar{\boldsymbol{f}}_*$, and $cov(\boldsymbol{f}_*)$ are the GP posterior prediction, its corresponding mean and its covariance, respectively; $K(X,X)$, $K(X_*,X_*)$, and $K(X,X_*)$ are the covariance matrices between training inputs, the testing inputs, and training and testing inputs, respectively; y is the training target vector, and σ_n is the noise variance.

5. Cycle ageing model

For an accurate prediction of Li-ion battery ageing at several static and dynamic conditions, it is of paramount importance to take into account the effect of the different stress factors influencing on the ageing mechanisms, and understand how they impact the capacity loss of Li-ion batteries. Under the GP framework, these tasks are traduced as a correct selection of the input and kernel functions.

5.1. Relating ageing mechanisms, model inputs and kernel functions

The selection of the structural form of the kernel is the most important challenge in nonparametric regression [8]. However, it remains a black art, as there is not any broadly accepted method to perform this task [9]. For most the GP ageing models presented in the literature, the selection of the kernel was based on trial and error methods, in which the kernel function presenting the lowest error was considered as the most suitable. Following this method, the suitability of the selected kernel in the general context of Li-ion battery ageing prediction could hardly be guaranteed, due to its high correlation to the used dataset. In order to develop GP models tailored to Li-ion battery ageing application, a stronger justification based on the prior knowledge on the expected ageing mechanisms is necessary for the appropriate selection of the kernel.

According to the literature, relatively high charging and discharging currents stimulate the cracking of the electrode particles. However, at lower current rates of battery operation the Solid Electrolyte Interface (SEI) cracking and reforming was proposed to be the main mechanism inducing capacity loss, without affecting the electrode particle itself [10]. Such capacity loss was shown to be proportional to the square of the state of lithiation swing (which could be approximated by the DOD) of the electrode particle, during lithiation [10]. The ageing data analysed in this study corresponds to relatively low C-rate values (C/3 charging and 1C discharging), which allows to assume a prior belief of a squared DOD dependence for the capacity loss.

Therefore, the squared-exponential kernel, which is able to handle all the projections into the space of powers [8], is considered to be suitable to host the DOD input dimension.

Besides, the capacity loss seems to have a U-shape dependency to the Middle-SOC, with an optimum around 50% SOC and stronger degradations at higher and lower cycling ranges [11]. As for the DOD input, the squared-exponential kernel should be an appropriate choice to capture such a squared Middle-SOC dependency. Furthermore, the growth of the SEI layer is a chemical reaction and then obeys to the Arrhenius law: the SEI formation rate increases exponentially with temperature. Such an exponential dependence, defined as the linear combination of an infinite number of power functions, could also be captured by the squared-exponential kernel.

Finally, a last input denoted ΔAh was defined as the Ah-throughput for which the capacity loss is desired to be predicted. Notice that, an isotropic kernel (e.g. squared-exponential) associated to such an input would require a large number of training ΔAh values to allow long term prediction, drastically increasing the size of the training dataset, as well as the computational cost of the model[1]. A linear anisotropic kernel was then selected for this input dimension. Summarising, the model proposed in this study considered four inputs:

- ΔAh: the Ah-throughput for which the ageing is desired to be predicted, modelled by a linear anisotropic kernel.
- T: the ambient temperature, modelled by a squared-exponential kernel.
- DoD: the DOD at which such ΔAh were cycled, modelled by a squared-exponential kernel.
- *Middle-SOC*: the average SOC corresponding to such DOD, modelled by a squared-exponential kernel.

The output of the model was the capacity loss ΔQ corresponding to the cycling of ΔAh.

5.2. Composing the whole kernel

As pointed out in Section 5.1, the model must be able to handle different input dimensions. Consequently, compositional kernels' framework seems to be a suitable solution to construct a main kernel composed of interpretable components, each one related to a specific input dimension [9]. In order to focus on the behaviour of the composed kernels, a zero-mean function was defined in this work. This is not a drastic limitation, since the mean of the posterior process is not confined to be zero [8].

In the GP framework, the kernel function is also a covariance function and then must be positive semidefinite [8]. Moreover, positive semidefinite compositional kernels are closed under addition and multiplication of basic kernels. Additive kernels assume the added stochastic processes to be independent [9]. According to the literature, the capacity loss corresponding to the SEI fracture results from a strong interaction between the temperature, DOD and Middle-SOC: the mechanical stress induced by both DOD and Middle-SOC leads to the SEI fracture, revealing this way a fresh anode surface to the electrolyte which give rise to the temperature dependent reforming of the SEI [10]. In order to account for the interactions between the different input dimensions, the tensor product is suggested [8,9]. The compositional kernel developed this way is expressed in equation (4).

$$\kappa(\mathrm{x},\mathrm{x}') = {\sigma_f}^2 \cdot \left[exp\left(-\frac{|x_1 - {x'}_1|^2}{2 \cdot {\theta_T}^2}\right) \cdot exp\left(-\frac{|x_2 - {x'}_2|^2}{2 \cdot {\theta_{DoD}}^2}\right) \cdot exp\left(-\frac{|x_3 - {x'}_3|^2}{2 \cdot {\theta_{Middle-SOC}}^2}\right) \cdot \left(x_4 \cdot {x'}_4 + {\theta_{\Delta Ah}}^2\right)\right] \tag{4}$$

where x and x′ are different input vectors structured as $\mathrm{x} = (x_1, x_2, x_3, x_4)$, with $x_1 = T^{-1}$, $x_2 = DoD$, $x_3 = Middle\text{-}SOC$, $x_4 = \Delta Ah$.

[1] More information about the properties of isotropic kernels in [8]

θ_T, θ_{DoD}, $\theta_{Middle\text{-}SOC}$ and $\theta_{\Delta t}$ are the hyperparameters related to the T, DoD, $Middle\text{-}SOC$ and ΔAh inputs respectively. The additional hyperparameter σ_f is the signal variance, and plays the role of scaling the outputs.

6. Results

Three different metrics were used to assess the prediction performances of the ageing models. The first one was the root-mean-square error (RMSE) of the output of the model, which was the capacity loss ΔQ, defined according to equation (5) - left. The second metric was the RMSE of the predicted capacity curve, expressed in equation (5) - right. This second metric is useful to evaluate the accumulative error of the model. The last metric was the calibration score and aimed at quantifying the accuracy of uncertainty estimates. It is defined as the percentage of measured results in the test dataset that are within a predicted credible interval. Within an $\pm 2\sigma$ interval, corresponding to a 95.4% probability for a Gaussian distribution, the calibration score is given by equation (6). Therefore, $CS_{2\sigma}$ should be approximately 95.4% if the uncertainty predictions are accurate. Higher or lower scores indicate under- or over-confidence, respectively.

$$RMSE_{\Delta Q}(\hat{y}_i, y_i) = \sqrt{\frac{1}{N_T}\sum_{i=1}^{N_T}(\hat{y}_i - y_i)^2} \qquad RMSE_Q(\hat{Q}_i, Q_i) = \sqrt{\frac{1}{N_T}\sum_{i=1}^{N_T}(\hat{Q}_i - Q_i)^2} \tag{5}$$

$$CS_{2\sigma} = \frac{1}{N_T}\sum_{i=1}^{N_T}[|\hat{y}_i - y_i| < 2\sigma] \cdot 100 \tag{6}$$

where $\hat{y}_i$ is the predicted output, y_i is the measured output, N_T is the number of points to be evaluated, $\hat{Q}_i$ is the predicted capacity calculated by accumulation of the output and Q_i is the measured capacity.

6.1. Learning from static conditions

In order to assess the performances of the model seven cases were studied, each one involving a different quantity of training data. From the CASE 1 to CASE 7, the ratio of the training data with respect to the whole dataset increases, and the range of different cycling temperature, DOD and Middle-SOC conditions observed during the training phase is broadened. The operating conditions involved in each cases were specifically selected to clearly illustrate the ability of the GP model to learn the influence of new stress-factor levels on the capacity loss. A 3% error threshold in terms of $RMSE_Q$ was established as accuracy criterion.

CASE 1 only comprised two different temperatures, a single DOD and Middle-SOC level. CASE 2 completed the temperature dimension with the observation of a third level. CASE 3 and 4 corresponded to the learning of the influence of DOD on the capacity loss, involving respectively two and three different DOD cycling levels. CASE 5 and 6 completed the model presenting an increasing number of Middle-SOC values, and CASE 7 included in the training dataset all the operating conditions available from the experimental ageing tests. The characteristics of each case are indicated in Table 2, specifying the different cells and the related operating conditions involved during the training process, as well as the corresponding ratio of the training data with respect to the whole available data. In each case, the GP model introduced in Section 5 was trained with the corresponding training cells, and the ageing was predicted for all the cells, in order to validate the generalisation capabilities of the obtained models. The maxima and average $RMSE$ and $CS_{2\sigma}$ values of all the tested cells are also indicated. The evolution of the metrics for each cell is represented in Figure 2.

Table 2. Summary of the different case studies and average and maxima metrics values obtained with the GP developed in Section 5, calculated from the predictions of all the cells. Best results are indicated in bold.

		CASE 1				CASE 2				CASE 3				CASE 4				CASE 5				CASE 6				CASE 7			
		Cell number	**Cycling conditions**			**Cell number**	**Cycling conditions**			**Cell number**	**Cycling conditions**			**Cell number**	**Cycling conditions**			**Cell number**	**Cycling conditions**			**Cell number**	**Cycling conditions**			**Cell number**	**Cycling conditions**		
			T	**DoD**	**MidSOC**		**T**	**DoD**	**MidSOC**		**T**	**DoD**	**MidSOC**		**T**	**DoD**	**MidSOC**		**T**	**DoD**	**MidSOC**		**T**	**DoD**	**MidSOC**		**T**	**DoD**	**MidSOC**
Training cells		CELL001-003	25	100	50	CELL001-003	25	100	50	CELL001-003	25	100	50	CELL001-003	25	100	50	CELL001-003	25	100	50	CELL001-003	25	100	50	all	all		
		CELL100-102	45	100	50	CELL100-102	45	100	50	CELL100-102	45	100	50	CELL100-102	45	100	50	CELL100-102	45	100	50	CELL100-102	45	100	50				
						CELL030-032	35	100	50	CELL030-032	35	100	50	CELL030-032	35	100	50	CELL030-032	35	100	50	CELL030-032	35	100	50				
										CELL021-022	25	20	50	CELL021-022	25	20	50	CELL021-022	25	20	50	CELL021-022	25	20	50				
										CELL120-122	45	20	50	CELL120-122	45	20	50	CELL120-122	45	20	50	CELL120-122	45	20	50				
										CELL067-069	35	20	50	CELL067-069	35	20	50	CELL067-069	35	20	50	CELL067-069	35	20	50				
														CELL015-017	25	50	50	CELL015-017	25	50	50	CELL015-017	25	50	50				
														CELL114-116	45	50	50	CELL114-116	45	50	50	CELL114-116	45	50	50				
														CELL047-054	35	50	50	CELL047-054	35	50	50	CELL047-054	35	50	50				
																		CELL073-075	35	20	20	CELL073-075	35	20	20				
																		CELL082-84	35	10	20	CELL082-84	35	10	20				
																						CELL061-063	35	20	80				
																						CELL076-078	35	10	80				
Training/Validation ratio [%]		9.38				12.51				19.49				39.45				43.15				51.58				100			
Performance metrics	**Maximum $RMSE_{\Delta Q}$ [%]**	2.86				**2.36**				2.38				2.38				2.38				2.38				2.38			
	Average $RMSE_{\Delta Q}$ [%]	1.12				0.95				0.82				0.72				0.70				**0.68**				0.70			
	Maximum $RMSE_{Q}$ [%]	8.46				5.85				3.90				**2.83**				**2.83**				**2.83**				3.46			
	Average $RMSE_{Q}$ [%]	2.82				2.22				1.75				1.15				1.09				**1.05**				1.11			
	Maximum $CS_{2\sigma}$ [%]	**100**				**100**				**100**				**100**				**100**				**100**				**100**			
	Minimum $CS_{2\sigma}$ [%]	19.35				**32.43**				10.71				0				0				0				0			
	Average $CS_{2\sigma}$ [%]	83.42				**93.63**				65.93				77.51				74.12				71.95				72.77			

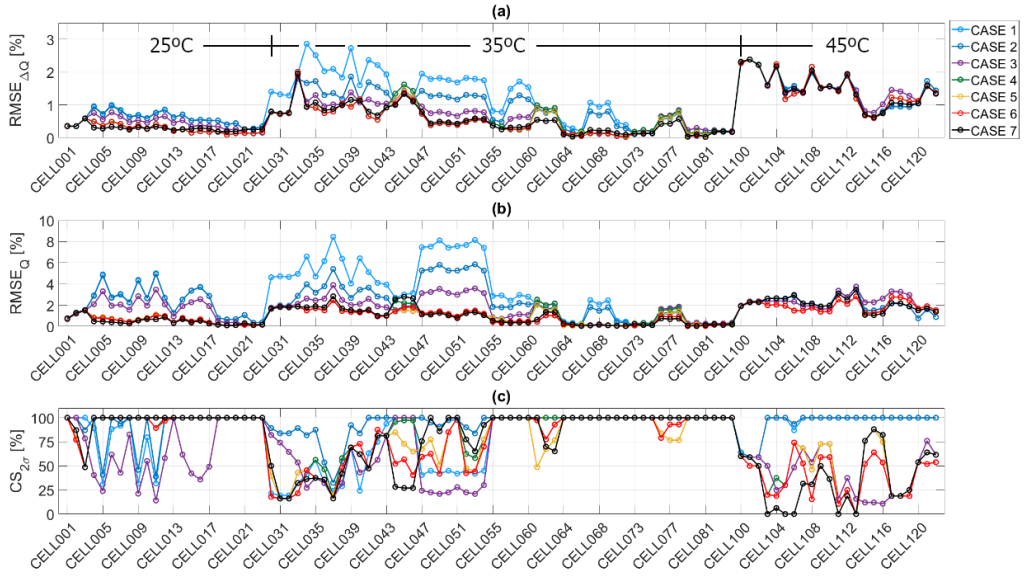

Figure 2. Evolution of the metrics over the different case studies with the model developed in Section 5, for all the cells tested at static cycling conditions.

The GP model trained in CASE 1 demonstrated poor prediction performances for most operating conditions involving a DOD level unobserved in training (see Figure 2.a-b). As expected, a clear improvement was observed in CASE 2 for all the cells cycling at 35°C, but the prediction errors at several DODs remained superior to the defined 3% threshold. With the introduction of a second DOD level in CASE 3, the model could perform a first fitting in the DOD dimension, and the extension to 50% DOD in CASE 4 allowed to achieve the 3% $RMSE_Q$ accuracy criterion for all the cells. In CASE 5 and 6, the data corresponding to low and high Middle-SOC cycling was incorporated in the training set, respectively. The improvement of prediction performances were in such cases limited (see cells 044-046, 061-063, 076-078 in Figure 2.b), due to the reduced impact of the Middle-SOC stress-factor compared to the cycling temperature and DOD. Finally, all the available data was included in the training set in CASE 7. Unexpectedly, the average $RMSE_{\Delta Q}$ and $RMSE_Q$ metrics which revealed reducing values from CASE1 to CASE 6, increased for the training CASE 7. This observation could possibly be explained by the coupled effect of i) a higher number of mismatches in the data, partially due to small deviations induced by procedural and measurement errors during the experimental testing, ii) the limited capability of the developed GP model to explain the data, due to the slight nonlinearities of the capacity curves in the Ah-throughput dimension, and iii) the saturation of the learning capabilities of the GP model, which limits the scope for reduction of the error metrics as most of the possible operating conditions were already observed.

Regarding the $CS_{2\sigma}$ metric (see Figure 2.c), a non-monotonic evolution was observable for the cells 030-54 and 100-122. This is also explainable by the linear character of the model´s predictions in the Ah-throughput dimension. Actually, such a cells present slightly nonlinear capacity curves, with a lower capacity loss in the beginning of life, then a faster linear trend, sometimes followed by a slowdown (see Figure 1). Besides, according to the equation (3), the predicted confidence boundaries reduce as the GP model is observing a larger number of operating conditions, indicating that the GP is becoming more confident. Therefore, more data samples remain out of the confidence boundaries, depending on the nonlinearities in the Ah-throughput dimension. This induces large variations in the evolution of the $CS_{2\sigma}$ metric, which clearly remained under the desired 95.4% value for all these cells, implying a strongly over-confident behaviour of the model. Oppositely, a clear convergence into 100% $CS_{2\sigma}$ was observable for the cells 001-023 and 055-084, indicating under-confident predictions for those cells. This is explainable by the particularly straight capacity curves observable for those cells, which, combined with the relatively high noise hyperparameter imposed by the cells presenting nonlinear capacity curves, leads to relatively large confidence boundaries that encompass all the data samples.

For many covariance functions, the observation of the hyperparameters allows to interpret how the GP model understand the data. As explained in [8], for the squared-exponential kernel, the hyperparameters play "*the*

rôle of characteristic length-scale. Such a covariance function implements automatic relevance determination (ARD), since the inverse of the length-scale determines how relevant an input is: if the length-scale has a very large value, the covariance will become almost independent of that input, effectively removing it from the inference". Figure 3 displays, for each case study, the inverse of the hyperparameters corresponding to each input dimension, relatively normalised to each other.

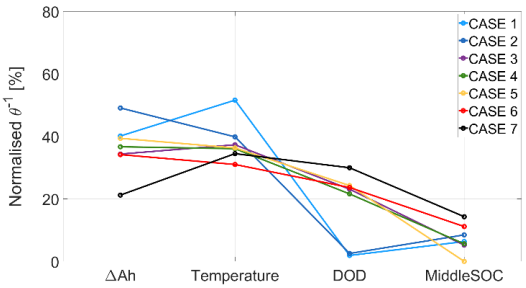

Figure 3. Inverse of the hyperparameters corresponding to each input dimension, relatively normalised to each other.

Notice that the interpretability of the hyperparameter of the ΔAh input is debatable, due to the anisotropic character of the corresponding kernel. However, the relative values of the inverse of Temperature, DOD and Middle-SOC inputs' hyperparameters indicate how relevant each stress-factor is with respect to the capacity loss. It is important to highlight that, although such comparison could clarify how the GP model understand the data, it does not imply causality. For CASE 1 and 2, the GP model considered the temperature input considerably more relevant than the DOD and Middle-SOC. However, at this stage, the training data only involved single DOD and Middle-SOC levels, hindering the inference in these dimensions, and the corresponding rates displayed in Figure 3 were "floating" values resulting from the optimisation. As CASE 3 and 4 involved different DOD values, the model allocated an increased importance to such input variations. In CASE 5, the inclusion of the data corresponding to 20% Middle-SOC removed the influence such stress factor from the GP model predictions: in fact, the capacity loss at low and medium Middle-SOC was similar in the experimental data, which led the model to deem this stress-factor completely unrelated with the capacity loss. Such estimation was corrected in CASE 6 and 7, to finally classify the relevance of the different stress-factors with respect to the capacity loss prediction in this order: 1/ temperature, 2/ DOD and 3/ Middle-SOC (the relation between the hyperparameter value and the "relevance" being debatable for ΔAh input).

The predictions of the developed GP model are illustrated for the cells cycled at 25°C, 80% DOD and 50% Middle-SOC, for the different cases.

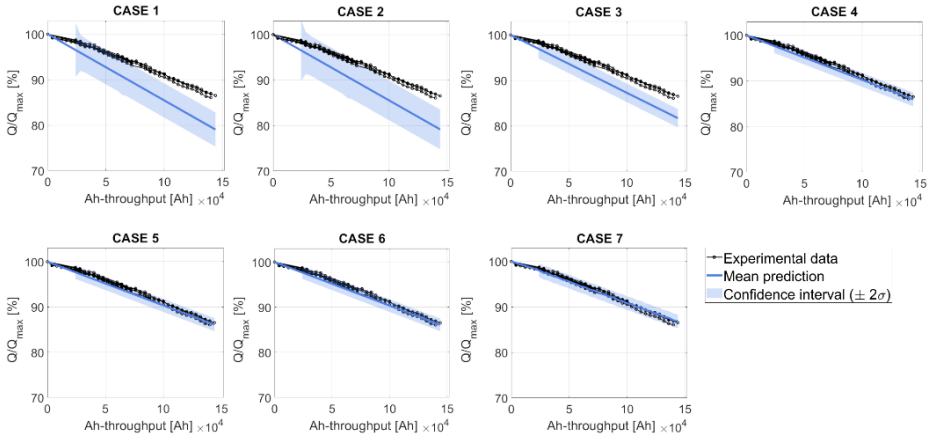

Figure 4. Predictions for the cells cycled at 25°C, 80% DOD and 50% Middle-SOC, for the different cases.

The model performed inaccurate and uncertain predictions for CASE 1 and 2, due to the single DOD value in the training data. The involvement of the 20% DOD and 50% DOD levels, respectively in CASE 3 and 4, allowed to improve the accuracy and uncertainty quantification of the model reaching an average of 1.21 $RMSE_Q$ and 95.31% $CS_{2\sigma}$ for these cells in CASE 4, which traduce a suitable understanding of the effect of the DOD on capacity loss. As expected, the observation of new Middle-SOC values in CASE 5 and 6 did not affect the results. In CASE 7, the data corresponding to the operating conditions under study were included

in the training set. However, the model prediction did not change significantly, suggesting a correct generalisation capability in the DOD dimension, for the model trained in CASE 4.

6.2. Learning from dynamic conditions

The operating conditions of Li-ion batteries are barely constant in real-world operation, and therefore the predictive capabilities of the ageing models need to be validated at dynamic operating conditions. In order to ensure the validity of the developed model to perform accurate predictions at dynamic operating conditions, and illustrate the ability to complete the model training from the observation of such dynamic profiles, 2 additional cells were submitted to dynamic temperature, DOD, Middle-SOC and C-rate profiles. The obtained capacity data and model's predictions, as well as the corresponding DOD, Middle-SOC, Temperature and C-rates profiles are displayed in Figure 5, for one of those cells.

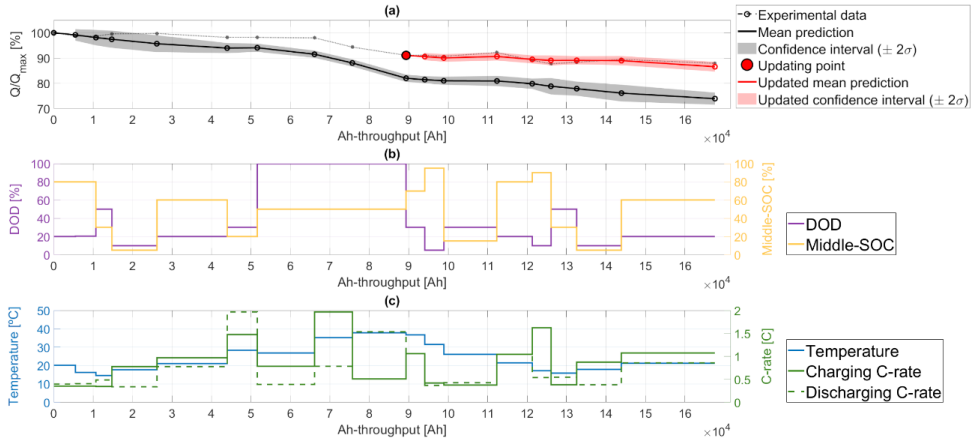

Figure 5. (a) Mean prediction and confidence intervals of the initial GP model (black line and grey area), and the updated model's predictions (red line and red area). (b) Dynamic DOD and Middle-SOC profiles. (c) Dynamic temperature and charging and discharging C-rates.

The GP model trained with the data corresponding to CASE 6 was selected for the dynamic validation. Actually, such model already observed different values for all the input dimensions, and it is expected to be able to correctly predict the capacity loss. In Figure 5.a, the initial model (black line and grey area) performed a clearly pessimistic prediction, mainly explained by i) the inability of the model to handle the slower capacity loss often observable in the BOL, and ii) the reduced capacity loss observed at 100% DoD (between 50000-90000 Ah-throughput range) compared with the static training data at the same static conditions.

At approximately 90000 Ah-throughput (≈ 50% of the data available for this cell), the observed data samples were included in the training dataset of the model, and a second prediction was performed from this point (red line and red area in Figure 5.a). The operating conditions between 10700-43960 Ah-throughput, which were included in the training phase, were repeated between 126000-167600 Ah-throughput. Such operating conditions were not observed in the initial training (CASE 6), and this allows to assess the learning capabilities of the model. Neglecting the shift corresponding to the initial point correction, the updated model provided a slightly smaller degradation compared to the initial prediction, in accordance the newly included training data. Furthermore, the confidence boundaries were reduced for such operating conditions, indicating a more confident behaviour of the updated model.

7. Discussion, limitations of the study and further works

In this study, the selection of the inputs and the corresponding kernel functions, as well as the composition of the whole kernel were based on the assumption that the SEI cracking and the subsequent SEI reformation were the main causes of the capacity loss, due to the relatively low charging and discharging C-rates used for the experimental data presented in Figure 1. However, real-world operation may involve higher C-rate values for both charging and discharging, and the ageing model presented in this study should be extended to take into consideration the different ageing mechanisms as the particle fracture and the lithium plating, which are stimulated by high C-rate levels. The sudden capacity drop phenomenon, sometimes related to the irreversible lithium plating mechanism, and the effect of the charging and discharging C-rates are also

planned to be considered in a further publication. Besides, the accuracy of the model presented in this study revealed to be limited by the inability of the model to fit nonlinearities in the Ah-throughput dimension, as explained in Section 6. This could be solved by the inclusion of an additional input e.g. the capacity value from which the prediction is performed. Finally, the ability of the model to learn from dynamic operating conditions deserves to be further investigated, in order to i) quantify better the number of experimental tests required at static ageing conditions and ii) identify the learning limitations from the dynamic operating profiles, induced by the path-dependence.

8. Conclusions

In this study, a self-adaptive capacity loss model was developed based on the Gaussian Process framework. The model was able to perform accurate predictions for a broad panel of temperature, DOD and Middle-SOC cycling conditions, reaching an average value of 1.15% $RMSE_Q$, with a reduced number of laboratory training tests (9 different conditions). The ability of the self-adaptive model to learn from the new data samples was demonstrated at both static and dynamic conditions.

Acknowledgments

This investigation work was financially supported by the RETOS Program (ReViBE project, TEC2015-63899-C3-2-R) of the Spanish Ministry of Economy, Industry and Competitiveness, as well as by ELKARTEK (CICe2018 - Desarrollo de actividades de investigación fundamental estratégica en almacenamiento de energiá electroquímica y térmica para sistemas de almadenamiento híbridos, KK-2018/00098) and EMAITEK Strategic Programs of the Basque Government.

References

[1] S. Dhundhara, Y.P. Verma, A. Williams, Techno-economic analysis of the lithium-ion and lead-acid battery in microgrid systems, Energy Convers. Manag. 177 (2018) 122–142. doi:10.1016/j.enconman.2018.09.030.

[2] M. Dubarry, N. Qin, P. Brooker, Calendar aging of commercial Li-ion cells of different chemistries – A review, Curr. Opin. Electrochem. 9 (2018) 106–113. doi:10.1016/j.coelec.2018.05.023.

[3] E. Sarasketa-Zabala, I. Gandiaga, E. Martinez-Laserna, L.M. Rodriguez-Martinez, I. Villarreal, Cycle ageing analysis of a LiFePO4/graphite cell with dynamic model validations: Towards realistic lifetime predictions, J. Power Sources. 275 (2015) 573–587. doi:10.1016/j.jpowsour.2014.10.153.

[4] E. Sarasketa-Zabala, E. Martinez-Laserna, M. Berecibar, I. Gandiaga, L.M. Rodriguez-Martinez, I. Villarreal, Realistic lifetime prediction approach for Li-ion batteries, Appl. Energy. 162 (2016) 839–852. doi:10.1016/j.apenergy.2015.10.115.

[5] M. Dubarry, G. Baure, A. Devie, Durability and Reliability of EV Batteries under Electric Utility Grid Operations: Path Dependence of Battery Degradation, J. Electrochem. Soc. 165 (2018) A773–A783. doi:10.1149/2.0421805jes.

[6] M. Lucu, E. Martinez-Laserna, I. Gandiaga, H. Camblong, A critical review on self-adaptive Li-ion battery ageing models, J. Power Sources. 401 (2018) 85–101. doi:10.1016/j.jpowsour.2018.08.064.

[7] M. Lewerenz, J. Münnix, J. Schmalstieg, S. Käbitz, M. Knips, D.U. Sauer, Systematic aging of commercial LiFePO 4 |Graphite cylindrical cells including a theory explaining rise of capacity during aging, J. Power Sources. 345 (2017) 254–263. doi:10.1016/j.jpowsour.2017.01.133.

[8] C.E. Rasmussen, C.K.I. Williams, Gaussian Processes for Machine Learning, MIT Press, 2005. http://www.gaussianprocess.org/gpml/chapters/RW.pdf.

[9] D. Duvenaud, J. Lloyd, R. Grosse, J. Tenenbaum, Z. Ghahramani, Structure Discovery in Nonparametric Regression through Compositional Kernel Search, Proc. Mach. Learn. Res. 28 (2013) 1166–1174. doi:10.1098/rsta.2010.0144.

[10] R.D. Deshpande, D.M. Bernardi, Modeling Solid-Electrolyte Interphase (SEI) Fracture: Coupled Mechanical/Chemical Degradation of the Lithium Ion Battery, J. Electrochem. Soc. 164 (2017) A461–A474. doi:10.1149/2.0841702jes.

[11] M. Ecker, N. Nieto, S. Käbitz, J. Schmalstieg, H. Blanke, A. Warnecke, D.U. Sauer, Calendar and cycle life

study of Li(NiMnCo)O2-based 18650 lithium-ion batteries, J. Power Sources. 248 (2014) 839–851. doi:10.1016/j.jpowsour.2013.09.143.

Authors

Mattin Lucu received his M.Sc in Integration of Renewable Energy Sources into the Electricity Grid from the University of the Basque Country, UPV-EHU (Spain) in 2016. During his graduate studies, he worked as R&D intern successively at EneR-GEA research group (ESTIA Engineering School, France) in wind turbine emulation and control, and at EDP in the analysis of photovoltaic power insertion in low-voltage distribution networks. In 2016, he joined the IK4-Ikerlan Technology Research Centre, where he is coursing a Ph.D. degree in collaboration with the University of the Basque Country. His research interests include electrochemical energy storage systems and machine learning algorithms applied to their lifetime estimation.

Jon Ander López-Ibarra received his Industrial Electrical Eng. degree and M.Sc in Integration of Renewable Energy Sources into Electricity Grid from the University of the Basque Country (UPV-EHU), Spain, in 2015 and 2017, respectively. He joined the Energy Business Unit of IK4-IKERLAN Technological Research Centre, Spain, in 2017, where he is coursing a Ph.D. degree, in collaboration with the University of the Basque Country (UPV-EHU), Spain. His research is focused on the development of strategies for improved energy management in fleets of vehicles. His research interests include electrochemical energy storage systems, hybrid and electric vehicles, energy management and electrification of transportation.

Dr. Eng. Egoitz Martinez Laserna was born in 1989 in Vitoria-Gasteiz. He received his M.Sc in Electronic Engineering from the University of Mondragon, Spain, in 2013. He joined the Energy Business Unit of IK4-IKERLAN Technological Research Centre, Spain, in 2013. He obtained his Ph.D. in Engineering with international mention in 2017, focused on 2nd life battery performance, sizing and integration. His research interests include electrochemical energy storage systems, electric vehicles, renewable energy, energy management and BMS hardware design. He has been co-author of various scientific publications and has contributed to multiple international conferences.

Iñigo Gandiaga received a Diploma in Physics from the University of the Basque Country, UPV-EHU (Spain) in 2010. He joined the Energy Business Unit of IK4-IKERLAN Technology Research Centre in 2010. His research interests include from the lifetime estimation and sizing studies of different electrochemical energy storage technologies (EDLC, Li-ion and NiMH) for heavy duty transport and stationary applications, to SOC/SOH estimation algorithms for lithium-ion Battery Management Systems. He has been coordinator of various research projects with different industrial partners such as CAF or General Electric.

Haritza Camblong received the Electr. Eng. degree from the ENSIEG, Grenoble, in 1996, and the Ph.D. degree in Control Eng. from ENSAM in 2003. After his graduation in 1996, he worked in Ikerlan research center for two years in mechatronics applications. Later, he worked with MSI engineering company for other two years. In 2001, he joined ESTIA Engineering School, where he created EneR-GEA research group of which he is scientific referent nowadays. Since November 2008, he is a member of the University of the Basque Country. He is currently with the Systems Engineering and Control Department, and SI+E research group in Donostia-San Sebastián. His current research interests include control of wind turbines, power electronics, smart grids and storage systems.